AIAA SciTech Forum
8–12 January 2018, Kissimmee, Florida
2018 AIAA Guidance, Navigation, and Control Conference

10.2514/6.2018-1115

Stability Analysis for Incremental Nonlinear Dynamic Inversion Control

Xuerui Wang*, Erik-Jan van Kampen†, Qiping Chu‡
Delft University of Technology, Delft, Zuid-Holland, 2629HS, The Netherlands

Peng Lu§
Eidgenössische Technische Hochschule Zürich, 8093 Zürich, Switzerland

As a sensor-based control approach, the Incremental Nonlinear Dynamic Inversion (INDI) method has been successfully applied on various aerospace systems and shown desirable robust performance to aerodynamic model uncertainties. However, its previous derivations based on the so-called time scale separation principle is not mathematically rigorous. There also lack of stability and robustness analysis for INDI. Therefore, this paper reformulated the INDI control law without using the time scale separation principle and generalized it to not necessarily relative-degree-one problems, with consideration of the internal dynamics. Besides, the stability of the closed-loop system in the presence of external disturbances is analyzed using Lyapunov methods and nonlinear system perturbation theory. Moreover, the robustness of the closed-loop system against regular and singular perturbations is analyzed. Finally, the reformulated INDI control law and main conclusions are verified by a rigid aircraft gust load alleviation problem.

I. Introduction

Nonlinear Dynamic Inversion (NDI) is a nonlinear control method which cancels the system nonlinearity by means of feedback and results into entirely or partly linearized closed-loop system dynamics, where conventional linear control techniques can then be applied [1, 2]. This method is essentially different from the widely used Jacobian linearization around specific operational points in combination with gain-scheduled linear controllers, whose stability and performance become questionable between operational points.

The NDI control method requires an accurate knowledge of the nonlinear system dynamics to achieve an explicit cancellation. Such requirement is almost impossible to meet in reality due to model simplifications, computational errors and parametric uncertainties. This main drawback of NDI control motived many control technologies to improve its robustness. One popular approach is combining NDI control with linear robust control techniques such as structural singular value (μ) analysis [3, 4] and $\mathcal{H}_\infty$ synthesis. Although these techniques have brought significant benefits to regular NDI, not all the uncertainties are taken into account or some known nonlinear, time-varying (NLTV) dynamics are treated as uncertainties, thus the closed-loop systems can be either marginally or overly conservative in performance and stability robustness [5].

There are many attempts on using indirect adaptive control methods to improve the robustness of NDI [6]. Indirect adaptive control methods, in some form or the other, rely on on-line identification, which requires on-line excitation and selection of thresholds. There are also some concerns about the stability and parameter convergence property of indirect adaptive NDI [6].

Incremental Nonlinear Dynamic Inversion (INDI) is a sensor-based control method, which requires less model information in both qualitative and quantitative sense, and thus improving the system robustness against model uncertainties. The concept of this method originated from the late nineties and was previously referred to as the Simplified NDI [7] and Modified NDI [8]. INDI control has been elaborately applied on various aerospace systems [9–17].

*PhD Candidate, Control and Simulation Section, Faculty of Aerospace Engineering, Delft University of Technology; Kluyverweg 1, 2629HS, Delft, The Netherlands. X.Wang-6@tudelft.nl.

†Assistant Professor, Control and Simulation Section, Faculty of Aerospace Engineering, Delft University of Technology; Kluyverweg 1, 2629HS, Delft, The Netherlands, E.vanKampen@tudelft.nl, Member AIAA.

‡Associate Professor, Control and Simulation Section, Faculty of Aerospace Engineering, Delft University of Technology; Kluyverweg 1, 2629HS, Delft, The Netherlands, Q.P.Chu@tudelft.nl, Member AIAA.

§Postdoctoral Researcher, Department of Mechanical and Process Engineering, ETH Zürich, pelu@ethz.ch.

Regarding its applications on aerospace systems, the INDI method is generally used for the inner loop angular velocity control [9–12], which leads to a relative-degree-one problem for each control channel. The internal dynamics are then avoided by using cascaded control structure, which is a common practice in rigid aircraft flight control designs [10, 11, 14]. However, the stability of the cascaded control structure is not easy to prove because of its dependency on the time scale separations between different control loops. Also, this cascaded control structure is not suitable for some problems. e.g. It is neither physically meaningful nor practical to separate the higher-order elastic dynamics into cascaded loops. In view of these reasons, the INDI control will be broadened into not necessarily relative-degree-one problems in this paper with consideration of the internal dynamics.

The existing derivations of the INDI control law are based on the so-called time scale separation principle, which claims that when the sampling frequency is high, the controls can change significantly faster than the states [9–17]. The nonlinear plants are then simplified into linear incremental dynamic equations by omitting state variation related nonlinear terms and higher-order terms in their Taylor series expansion, based on which the incremental control inputs are designed. This approach is not mathematically rigorous since the plant simplification is made before introducing the INDI control inputs and thus becomes deficient for unstable plants. Moreover, although the state related nonlinear terms and higher-order terms are not used in the INDI controller design, they should be kept in the closed-loop dynamic equations and remain influencing the closed-loop system stability and performance, which is also not the case in the existing derivations. Therefore, in this paper, the INDI control law will be reformulated without using the time scale separation principle, and the influences of the omitted terms will be analyzed using Lyapunov methods and nonlinear system perturbation theory [2].

Although INDI control has shown promising capability of external disturbance rejection [13–15], there is no theoretical proof so far for the stability of the closed-loop system under the perturbation of external disturbances. Also, the influences of disturbances on the internal dynamics remain unknown. These issues will also be addressed in the present paper.

Furthermore, in spite of the desirable robust performance of INDI to aerodynamic model uncertainties that has been verified via numerical simulations [9, 15], its previous theoretical stability and robustness proofs have some drawbacks. These previous attempts usually draw the stability conclusions based on the linear transfer functions derived from block diagrams [9, 13, 14], where inappropriate assumptions are made. The robust performance of this control method will be rediscussed in this paper, and comparisons with regular NDI method will also be made.

This paper is structured as follows: Sec. II reformulates the INDI control law for three different problems. The stability and robustness issues of INDI is discussed in Sec. III. Sec. IV provides a numerical example. Main conclusions and recommendations are presented in Sec. V.

II. Incremental Nonlinear Dynamic Inversion

In this section, the Incremental Nonlinear Dynamic Inversion (INDI) control method will be reformulated for three problems, namely the multi-input/multi-output (MIMO) input-output linearization, output tracking and input-to-state linearization in the presence of external disturbances.

A. MIMO Input-Output Linearization

Consider a MIMO nonlinear system described by

$$\begin{aligned} \dot{\boldsymbol{x}} &= \boldsymbol{f}(\boldsymbol{x}) + \boldsymbol{G}(\boldsymbol{x})\boldsymbol{u} \\ \boldsymbol{y} &= \boldsymbol{h}(\boldsymbol{x}) \end{aligned} \tag{1}$$

where $\boldsymbol{f} : \mathbb{R}^n \to \mathbb{R}^n$ and $\boldsymbol{h} : \mathbb{R}^n \to \mathbb{R}^p$ are smooth vector fields. $\boldsymbol{G}$ is a smooth function mapping $\mathbb{R}^n \to \mathbb{R}^{n\times m}$, whose columns are smooth vector fields. When $p < m$, which means the number of outputs is smaller than the number of inputs, control of the system given by Eq. (1) via input-output linearization method is an overdetermined problem, where a control allocation technique is needed. On the other hand, $p > m$ yields an underdetermined problem, and weighted least squares method can be used for the controller design, but the desired control aims cannot be fully achieved. $p = m$ is assumed in the following derivations.

Denote the elements of $\boldsymbol{h}$ as $h_i,\ i = 1, 2, ..., m$, and the column vectors of the matrix $\boldsymbol{G}$ as $\boldsymbol{g}_j,\ j = 1, 2, ..., m$, then the Lie derivatives [2] of the function h_i with respect to the vector fields $\boldsymbol{f}$ and $\boldsymbol{g}_j$ are defined as

$$\mathcal{L}_f h_i = \frac{\partial h_i}{\partial \boldsymbol{x}}\boldsymbol{f}, \quad \mathcal{L}_{g_j} h_i = \frac{\partial h_i}{\partial \boldsymbol{x}}\boldsymbol{g}_j, \quad \mathcal{L}_f^k h_i = \frac{\partial(\mathcal{L}_f^{k-1} h_i)}{\partial \boldsymbol{x}}\boldsymbol{f}, \quad \mathcal{L}_{g_j}\mathcal{L}_f^k h_i = \frac{\partial(\mathcal{L}_f^k h_i)}{\partial \boldsymbol{x}}\boldsymbol{g}_j \tag{2}$$

The relative degree ρ_i for each output channel i is defined as the smallest integer such that for all $\boldsymbol{x} \in \mathbb{R}^n$, at least one $j \in \{1, 2, ..., m\}$ satisfies $\mathcal{L}_{g_j}\mathcal{L}_f^{\rho_i - 1} h_i \neq 0$.

Define the vector relative degree [18] of the system as $\boldsymbol{\rho} = [\rho_1, \rho_2, ..., \rho_m]^T$ satisfying

$$\rho = \|\boldsymbol{\rho}\|_1 = \sum_{i=1}^{m} \rho_i \leq n \tag{3}$$

then the output dynamics of the system can be represented as

$$\begin{bmatrix} y_1^{(\rho_1)} \\ y_2^{(\rho_2)} \\ \vdots \\ y_m^{(\rho_m)} \end{bmatrix} = \begin{bmatrix} \mathcal{L}_f^{\rho_1} h_1(\boldsymbol{x}) \\ \mathcal{L}_f^{\rho_2} h_2(\boldsymbol{x}) \\ \vdots \\ \mathcal{L}_f^{\rho_m} h_m(\boldsymbol{x}) \end{bmatrix} + \begin{bmatrix} \mathcal{L}_{g_1}\mathcal{L}_f^{\rho_1 - 1} h_1(\boldsymbol{x}) & \mathcal{L}_{g_2}\mathcal{L}_f^{\rho_1 - 1} h_1(\boldsymbol{x}) & \cdots \mathcal{L}_{g_m}\mathcal{L}_f^{\rho_1 - 1} h_1(\boldsymbol{x}) \\ \mathcal{L}_{g_1}\mathcal{L}_f^{\rho_2 - 1} h_2(\boldsymbol{x}) & \mathcal{L}_{g_2}\mathcal{L}_f^{\rho_2 - 1} h_2(\boldsymbol{x}) & \cdots \mathcal{L}_{g_m}\mathcal{L}_f^{\rho_2 - 1} h_2(\boldsymbol{x}) \\ \vdots & \vdots & \vdots \\ \mathcal{L}_{g_1}\mathcal{L}_f^{\rho_m - 1} h_m(\boldsymbol{x}) & \mathcal{L}_{g_2}\mathcal{L}_f^{\rho_m - 1} h_m(\boldsymbol{x}) & \cdots \mathcal{L}_{g_m}\mathcal{L}_f^{\rho_m - 1} h_m(\boldsymbol{x}) \end{bmatrix} \boldsymbol{u} \tag{4}$$

or

$$\boldsymbol{y}^{(\boldsymbol{\rho})} = \boldsymbol{\alpha}(\boldsymbol{x}) + \mathcal{B}(\boldsymbol{x})\boldsymbol{u} \tag{5}$$

If $\rho = n$, then the system given by Eq. (1) is full-state feedback linearizable. Otherwise, there are $n - \rho$ internal dynamics unobservable from the output $\boldsymbol{y}$. According to the Frobenius theorem [2], $\forall \boldsymbol{x}_* \in D$, there exist smooth functions $\boldsymbol{\phi}(\boldsymbol{x}) = [\phi_1(\boldsymbol{x}), \phi_2(\boldsymbol{x}), ..., \phi_{n-\rho}(\boldsymbol{x})]^T$ defined in a neighborhood D_0 of $\boldsymbol{x}_*$ such that

$$\frac{\partial \phi_k}{\partial \boldsymbol{x}} \boldsymbol{g}_j(\boldsymbol{x}) = 0, \quad \forall k \in \{1, 2, ..., n - \rho\}, \quad \forall j \in \{1, 2, ..., m\}, \quad \forall \boldsymbol{x} \in D_0 \tag{6}$$

Also, $\boldsymbol{z} = \boldsymbol{T}(\boldsymbol{x})$ defined by

$$\begin{aligned} \boldsymbol{z} &= \boldsymbol{T}(\boldsymbol{x}) = [\boldsymbol{T}_1(\boldsymbol{x}); \boldsymbol{T}_2(\boldsymbol{x})] = [\boldsymbol{\eta}; \boldsymbol{\xi}], \quad \boldsymbol{\eta} = \boldsymbol{\phi}(\boldsymbol{x}), \quad \boldsymbol{\xi} = [\boldsymbol{\xi}_1; \boldsymbol{\xi}_2; ...; \boldsymbol{\xi}_m], \\ \boldsymbol{\xi}_i &= [h_i(\boldsymbol{x}), \mathcal{L}_f h_i(\boldsymbol{x}), ..., \mathcal{L}_f^{\rho_i - 1} h_i(\boldsymbol{x})]^T, \quad i = 1, 2, ..., m \end{aligned} \tag{7}$$

is a diffeomorphism on the domain D_0. $\boldsymbol{\eta}$ and $\boldsymbol{\xi}$ are the state vectors for the internal and external dynamics respectively. Using Eqs. (5, 6, 7), the nonlinear system described by Eq. (1) can be transformed into

$$\begin{aligned} \dot{\boldsymbol{\eta}} &= \boldsymbol{f}_0(\boldsymbol{\eta}, \boldsymbol{\xi}) = \frac{\partial \boldsymbol{\phi}}{\partial \boldsymbol{x}} \boldsymbol{f}(\boldsymbol{x}) \Big|_{\boldsymbol{x} = \boldsymbol{T}^{-1}(\boldsymbol{z})} \\ \dot{\boldsymbol{\xi}} &= \boldsymbol{A}_c \boldsymbol{\xi} + \boldsymbol{B}_c [\boldsymbol{\alpha}(\boldsymbol{x}) + \mathcal{B}(\boldsymbol{x})\boldsymbol{u}] \\ \boldsymbol{y} &= \boldsymbol{C}_c \boldsymbol{\xi} \end{aligned} \tag{8}$$

where $\boldsymbol{A}_c = \text{diag}\{\boldsymbol{A}_0^i\}$, $\boldsymbol{B}_c = \text{diag}\{\boldsymbol{B}_0^i\}$, $\boldsymbol{C}_c = \text{diag}\{\boldsymbol{C}_0^i\}$, $i = 1, 2, ..., m$, and $(\boldsymbol{A}_0^i, \boldsymbol{B}_0^i, \boldsymbol{C}_0^i)$ is a canonical form representation of a chain of ρ_i integrators.

Assume $\det\{\mathcal{B}(\boldsymbol{x})\} \neq 0$ (Otherwise, even $p = m$, it is still an underdetermined problem), the Nonlinear Dynamic Inversion (NDI) control law is designed as $\boldsymbol{u} = \mathcal{B}^{-1}(\boldsymbol{x})(\boldsymbol{\nu} - \boldsymbol{\alpha}(\boldsymbol{x}))$, where $\boldsymbol{\nu} \in \mathbb{R}^m$ is called the pseudo-control input. In the absence of model uncertainties and disturbances, this control law results in the closed-loop system

$$\begin{aligned} \dot{\boldsymbol{\eta}} &= \boldsymbol{f}_0(\boldsymbol{\eta}, \boldsymbol{\xi}) \\ \dot{\boldsymbol{\xi}} &= \boldsymbol{A}_c \boldsymbol{\xi} + \boldsymbol{B}_c \boldsymbol{\nu} \\ \boldsymbol{y} &= \boldsymbol{C}_c \boldsymbol{\xi} \end{aligned} \tag{9}$$

which indicates that the closed-loop system has $n - \rho$ internal dynamics, and m decoupled channels. The input-output mapping for each channel from ν_i to y_i is a chain of ρ_i integrators.

NDI control however is based on the exact mathematical cancellation of the nonlinear terms $\boldsymbol{\alpha}(\boldsymbol{x})$ and $\mathcal{B}(\boldsymbol{x})$. This is almost impossible in practice due to model simplifications, computational errors and parametric uncertainties. One method to reduce the control law model dependency is Incremental Nonlinear Dynamic Inversion (INDI) control, which

is derived by taking the first order Taylor series expansion of Eq. (5) around the current (denoted by the subscript 0) states $\boldsymbol{x}_0$ and control input $\boldsymbol{u}_0$ as

$$\begin{aligned}\boldsymbol{y}^{(\boldsymbol{\rho})} &= \boldsymbol{\alpha}(\boldsymbol{x}) + \mathcal{B}(\boldsymbol{x})\boldsymbol{u} \\ &= \boldsymbol{y}_0^{(\boldsymbol{\rho})} + \left.\frac{\partial[\boldsymbol{\alpha}(\boldsymbol{x}) + \mathcal{B}(\boldsymbol{x})\boldsymbol{u}]}{\partial \boldsymbol{x}}\right|_0 \Delta\boldsymbol{x} + \mathcal{B}(\boldsymbol{x}_0)\Delta\boldsymbol{u} + O(\Delta\boldsymbol{x}^2) \\ &= \boldsymbol{y}_0^{(\boldsymbol{\rho})} + \mathcal{B}(\boldsymbol{x}_0)\Delta\boldsymbol{u} + \boldsymbol{\delta}(z, \Delta t)\end{aligned} \tag{10}$$

where $\Delta\boldsymbol{x}$ and $\Delta\boldsymbol{u}$ represent the state and control increments in one sampling time step Δt. $\boldsymbol{\delta}(z, \Delta t)$ is given by

$$\boldsymbol{\delta}(z, \Delta t) = \left[\left.\frac{\partial[\boldsymbol{\alpha}(\boldsymbol{x}) + \mathcal{B}(\boldsymbol{x})\boldsymbol{u}]}{\partial \boldsymbol{x}}\right|_0 \Delta\boldsymbol{x} + O(\Delta\boldsymbol{x}^2)\right]\Bigg|_{\boldsymbol{x}=\boldsymbol{T}^{-1}(z)} \tag{11}$$

Design the incremental control input as

$$\Delta\boldsymbol{u} = \mathcal{B}(\boldsymbol{x}_0)^{-1}(\boldsymbol{\nu} - \boldsymbol{y}_0^{(\boldsymbol{\rho})}) \tag{12}$$

where $\boldsymbol{y}_0^{(\boldsymbol{\rho})}$ is measured or estimated. The total control command for the actuator is $\boldsymbol{u} = \boldsymbol{u}_0 + \Delta\boldsymbol{u}$. Substituting Eq. (12) into Eq. (10) results in the input-output mapping of $\boldsymbol{y}^{(\boldsymbol{\rho})} = \boldsymbol{\nu} + \boldsymbol{\delta}(z, \Delta t)$. Using the same diffeomorphism $z = \boldsymbol{T}(\boldsymbol{x})$, the closed-loop system dynamics under INDI control are given by

$$\begin{aligned}\dot{\boldsymbol{\eta}} &= \boldsymbol{f}_0(\boldsymbol{\eta}, \boldsymbol{\xi}) \\ \dot{\boldsymbol{\xi}} &= \boldsymbol{A}_c\boldsymbol{\xi} + \boldsymbol{B}_c[\boldsymbol{\nu} + \boldsymbol{\delta}(z, \Delta t)] \\ \boldsymbol{y} &= \boldsymbol{C}_c\boldsymbol{\xi}\end{aligned} \tag{13}$$

which is consistent with Eq. (9) except for the perturbation term $\boldsymbol{\delta}(z, \Delta t)$. Since $\boldsymbol{x}$ is continuously differentiable, the norm value of $\boldsymbol{\delta}(z, \Delta t)$ can be reduced by increasing the sampling frequency. The influence of the $\boldsymbol{\delta}(z, \Delta t)$ term on system stability and robustness will be analyzed in Sec. III. Although Eq. (9) under NDI control seems to be neat, perturbation terms will appear when model uncertainties are considered, which will also be shown in Sec. III. As compared to the conventional NDI control law, the INDI control method is less sensitive to model mismatches, because the model information of $\boldsymbol{\alpha}(\boldsymbol{x})$ is not used in Eq. (12). On the other hand, this INDI control law needs the measurement or estimation of $\boldsymbol{y}_0^{(\boldsymbol{\rho})}$ and the actuator position $\boldsymbol{u}_0$, this is why INDI control is referred to as a sensor-based approach.

B. Output Tracking

The INDI control law can also solve the command tracking problem. Consider the nonlinear plant (Eq. (1)) with relative degree $\boldsymbol{\rho} = [\rho_1, \rho_2, ..., \rho_m]^T$, which can be transformed into the internal and external dynamics given by Eq. (8). The output tracking problem requires the output $\boldsymbol{y}$ to asymptotically track a reference signal $\boldsymbol{r}(t) = [r_1(t), r_2(t), ..., r_m(t)]^T$. Assume $r_i(t), i = 1, 2, ..., m$ and its derivatives up to $r_i^{(\rho_i)}(t)$ are bounded for all t and $r_i^{(\rho_i)}(t)$ is piecewise continuous.

Denote the reference and the tracking error vectors as

$$\mathcal{R} = [\mathcal{R}_1; \mathcal{R}_2; ...; \mathcal{R}_m], \quad \mathcal{R}_i = [r_i, r_i^{(1)}, ..., r_i^{(\rho_i - 1)}]^T, \quad i = 1, 2, ..., m, \quad \boldsymbol{e} = \boldsymbol{\xi} - \mathcal{R} \tag{14}$$

Then Eq. (8) can then be transformed into

$$\begin{aligned}\dot{\boldsymbol{\eta}} &= \boldsymbol{f}_0(\boldsymbol{\eta}, \boldsymbol{e} + \mathcal{R}) \\ \dot{\boldsymbol{e}} &= \boldsymbol{A}_c\boldsymbol{e} + \boldsymbol{A}_c\mathcal{R} - \dot{\mathcal{R}} + \boldsymbol{B}_c[\boldsymbol{\alpha}(\boldsymbol{x}) + \mathcal{B}(\boldsymbol{x})\boldsymbol{u}] \\ &= \boldsymbol{A}_c\boldsymbol{e} + \boldsymbol{B}_c[\boldsymbol{\alpha}(\boldsymbol{x}) + \mathcal{B}(\boldsymbol{x})\boldsymbol{u} - \boldsymbol{r}^{(\boldsymbol{\rho})}]\end{aligned} \tag{15}$$

where $\boldsymbol{r}^{(\boldsymbol{\rho})} = [r_1^{(\rho_1)}, r_2^{(\rho_2)}, ..., r_m^{(\rho_m)}]^T$. The NDI control law is designed as

$$\boldsymbol{u} = \mathcal{B}^{-1}(\boldsymbol{x})[\boldsymbol{\nu} - \boldsymbol{\alpha}(\boldsymbol{x}) + \boldsymbol{r}^{(\boldsymbol{\rho})}] \tag{16}$$

When prefect model cancellation is assumed, this NDI control law results in the closed-loop system

$$\dot{\boldsymbol{\eta}} = \boldsymbol{f}_0(\boldsymbol{\eta}, \boldsymbol{e} + \mathcal{R}), \quad \dot{\boldsymbol{e}} = \boldsymbol{A}_c\boldsymbol{e} + \boldsymbol{B}_c\boldsymbol{\nu} \tag{17}$$

On the other hand, by using Eq. (10), the INDI control law can be designed as

$$\Delta \boldsymbol{u} = \mathcal{B}(\boldsymbol{x}_0)^{-1}[\boldsymbol{\nu} - \boldsymbol{y}_0^{(\boldsymbol{\rho})} + \boldsymbol{r}^{(\boldsymbol{\rho})}] \tag{18}$$

which leads to the closed-loop system as

$$\dot{\boldsymbol{\eta}} = \boldsymbol{f}_0(\boldsymbol{\eta}, \boldsymbol{e} + \mathcal{R}), \quad \dot{\boldsymbol{e}} = \boldsymbol{A}_c \boldsymbol{e} + \boldsymbol{B}_c[\boldsymbol{\nu} + \boldsymbol{\delta}(z, \Delta t)] \tag{19}$$

The closed-loop system dynamics given by Eq. (13) for the input-output linearization problem and the reference tracking problem described by Eq. (19) are essentially the same. Only the equilibrium point of $\boldsymbol{z} = [\boldsymbol{\eta}; \boldsymbol{\xi}] = \boldsymbol{0}$ is shifted into $\boldsymbol{z}' = [\boldsymbol{\eta}; \boldsymbol{e}] = \boldsymbol{0}$, so similar stability and robustness analyses can be made for these two problems.

C. Input-to-State Linearization under Disturbance Perturbations

Consider a special case of Input-output linearization by taking the outputs as $y_i = h_i(x) = x_i - x_{i*}, \ \ i = 1, 2, ..., m$, or equally $\boldsymbol{y} = \boldsymbol{H}(\boldsymbol{x} - \boldsymbol{x}_*)$, where $\boldsymbol{H}$ is a Boolean selection matrix and $\boldsymbol{x}_*$ is the equilibrium point. This choice of output results in a so-called *symmetrical system* [18] where all the m channels have the same relative degree $\rho_i = 1$, and the total relative degree is $\rho = m$. When $m < n$, there are $n - m$ internal dynamics.

Adding the disturbance perturbation $\boldsymbol{d} \in \mathbb{R}^n$ into the nonlinear plant (Eq. (1)) as

$$\begin{aligned} \dot{\boldsymbol{x}} &= \boldsymbol{f}(\boldsymbol{x}) + \boldsymbol{G}(\boldsymbol{x})\boldsymbol{u} + \boldsymbol{d} \\ \boldsymbol{y} &= \boldsymbol{H}(\boldsymbol{x} - \boldsymbol{x}_*) \end{aligned} \tag{20}$$

Recall Eq. (7), since $\rho_i = 1$, the external states are given by $\xi_i = h_i(x) = x_i - x_{i*}, \ i = 1, 2, .., m$ with dynamics

$$\dot{\boldsymbol{y}} = \dot{\boldsymbol{\xi}} = \bar{\boldsymbol{f}}(\boldsymbol{\xi}) + \bar{\boldsymbol{G}}(\boldsymbol{\xi})\boldsymbol{u} + \boldsymbol{H}\boldsymbol{d} \tag{21}$$

where $\bar{\boldsymbol{f}} : \mathbb{R}^\rho \to \mathbb{R}^m$, $\bar{\boldsymbol{g}} : \mathbb{R}^\rho \to \mathbb{R}^{m \times m}$ can be calculated by substituting $x_i = \xi_i + x_{i*}, \ i = 1, 2, ..., m$ into Eq. (20). Taking the first order Taylor series expansion of the external dynamic equations as

$$\begin{aligned} \dot{\boldsymbol{\xi}} &= \bar{\boldsymbol{f}}(\boldsymbol{\xi}) + \bar{\boldsymbol{G}}(\boldsymbol{\xi})\boldsymbol{u} + \boldsymbol{H}\boldsymbol{d} \\ &= \dot{\boldsymbol{\xi}}_0 + \frac{\partial[\bar{\boldsymbol{f}}(\boldsymbol{\xi}) + \bar{\boldsymbol{G}}(\boldsymbol{\xi})\boldsymbol{u}]}{\partial \boldsymbol{\xi}}\bigg|_0 \Delta\boldsymbol{\xi} + \bar{\boldsymbol{G}}(\boldsymbol{\xi}_0)\Delta\boldsymbol{u} + \boldsymbol{H}\Delta\boldsymbol{d} + O(\Delta\boldsymbol{\xi}^2) \\ &= \dot{\boldsymbol{\xi}}_0 + \bar{\boldsymbol{G}}(\boldsymbol{\xi}_0)\Delta\boldsymbol{u} + \boldsymbol{H}\Delta\boldsymbol{d} + \boldsymbol{\delta}(\boldsymbol{\xi}, \Delta t) \end{aligned} \tag{22}$$

Design the incremental control law as $\Delta\boldsymbol{u} = \bar{\boldsymbol{G}}^{-1}(\boldsymbol{\xi}_0)(\boldsymbol{\nu} - \dot{\boldsymbol{\xi}}_0)$, the closed-loop external dynamics are formulated by

$$\dot{\boldsymbol{\xi}} = \boldsymbol{\nu} + \boldsymbol{H}\Delta\boldsymbol{d} + \boldsymbol{\delta}(\boldsymbol{\xi}, \Delta t) \tag{23}$$

Analogously, using Eq. (6), the internal dynamics under disturbance perturbations are given by

$$\dot{\boldsymbol{\eta}} = \frac{\partial \boldsymbol{\phi}}{\partial \boldsymbol{x}}(\boldsymbol{f}(\boldsymbol{x}) + \boldsymbol{G}(\boldsymbol{x})\boldsymbol{u} + \boldsymbol{d}) = \frac{\partial \boldsymbol{\phi}}{\partial \boldsymbol{x}}(\boldsymbol{f}(\boldsymbol{x}) + \boldsymbol{d}) = \boldsymbol{f}_d(\boldsymbol{\eta}, \boldsymbol{\xi}, \boldsymbol{d}) \tag{24}$$

where $\boldsymbol{f}_d(\boldsymbol{\eta}, \boldsymbol{\xi}, \boldsymbol{d}) : \mathbb{R}^{n-\rho} \times \mathbb{R}^\rho \times \mathbb{R}^n \to \mathbb{R}^{n-\rho}$. Choose $\boldsymbol{\phi}(\boldsymbol{x}_*) = \boldsymbol{0}$, the diffeomorphism $\boldsymbol{z} = \boldsymbol{T}(\boldsymbol{x}) = [\boldsymbol{\eta}; \boldsymbol{\xi}]$ transforms the equilibrium $\boldsymbol{x} = \boldsymbol{x}_*$ into the origin point $\boldsymbol{z} = [\boldsymbol{\eta}; \boldsymbol{\xi}] = \boldsymbol{0}$.

When $\boldsymbol{d} = \boldsymbol{0}$, the input-to-state linearized closed-loop system dynamics given by Eqs. (23, 24) are a special case of the input-output linearized dynamics described by Eq. (13). It can also be observed from Eqs. (23, 24) that the disturbance $\boldsymbol{d}$ influences the external dynamics only by its increments $\Delta\boldsymbol{d}$ while directly influencing the internal dynamics. When the sampling frequency is sufficiently high, the disturbance increments $\|\Delta\boldsymbol{d}\|_2$ is smaller than $\|\boldsymbol{d}\|_2$. This is another feature of INDI control that the major part of the disturbance influences can be reflected in the measurement of $\dot{\boldsymbol{\xi}}_0$ and been compensated by the controller. This control method thus presents improved disturbance rejection ability as verified by simulations [15] and flight tests [13, 14]. This ability will be further analyzed in Sec. III.

III. Stability and Robustness Analysis

The stability and robustness of the present INDI control will be analyzed in this section. In the first subsection, the influences of the state variation related terms on closed-loop system stability will be discussed. The second subsection discusses the system robustness to regular and singular perturbations.

A. Stability Analysis

In this section, the stability of the origin $\boldsymbol{z} = \boldsymbol{0}$ of closed-loop system given by Eq. (13) under INDI control will be analyzed. Similar conclusions can be drawn for systems modeled by Eq. (19) and Eqs. (23, 24) without disturbances. The closed-loop system with external disturbances and model uncertainties will be analyzed in the next subsection. The proofs in this section also assume ideal actuator and perfect sensing. The actuator dynamics, nonlinear limits of actuators and the sensing issues will be discussed in the next subsection.

Design the pseudo-control $\boldsymbol{\nu} = -\boldsymbol{K}\boldsymbol{\xi}$ such that $\boldsymbol{A}_c - \boldsymbol{B}_c\boldsymbol{K}$ is Hurwitz, Eq. (13) results in

$$\begin{aligned} \dot{\boldsymbol{\eta}} &= \boldsymbol{f}_0(\boldsymbol{\eta}, \boldsymbol{\xi}) \\ \dot{\boldsymbol{\xi}} &= (\boldsymbol{A}_c - \boldsymbol{B}_c\boldsymbol{K})\boldsymbol{\xi} + \boldsymbol{B}_c\boldsymbol{\delta}(z, \Delta t) \end{aligned} \tag{25}$$

where the output equation is dropped since it plays no role in the stabilization problem.

Remark: The term $\boldsymbol{\delta}(z, \Delta t)$ in Eq. (10) or the term $\boldsymbol{\delta}(\boldsymbol{\xi}, \Delta t)$ in Eq. (22) are often directly omitted in literature [9–17] by claiming that the $\Delta\boldsymbol{\xi}$ related term is smaller than the $\Delta\boldsymbol{u}$ related term when the sampling frequency is high, which is referred to as the time scale separation principle. This statement is not mathematically rigorous and is especially deficient for unstable nonlinear plants because the plant simplifications are made before designing the INDI control inputs. Besides, although these terms are dropped out for the convenience of the controller design, they should be kept in the closed-loop system equations and remain influencing the closed-loop system stability and performance, which has been overlooked in literature.

Referring the following system as the *nominal system*

$$\begin{aligned} \dot{\boldsymbol{\eta}} &= \boldsymbol{f}_0(\boldsymbol{\eta}, \boldsymbol{\xi}) \\ \dot{\boldsymbol{\xi}} &= (\boldsymbol{A}_c - \boldsymbol{B}_c\boldsymbol{K})\boldsymbol{\xi} \end{aligned} \tag{26}$$

whose stability has been extensively proved in literature, and is listed here for completeness.

Lemma A.1 *The origin of Eq. (26) is asymptotically stable if the origin of* $\dot{\boldsymbol{\eta}} = \boldsymbol{f}_0(\boldsymbol{\eta}, \boldsymbol{0})$ *is asymptotically stable.*

$\dot{\boldsymbol{\eta}} = \boldsymbol{f}_0(\boldsymbol{\eta}, \boldsymbol{0})$ is referred to as the *zero dynamics*, and the nonlinear system is said to be *minimum phase* if its zero dynamics has an asymptotically stable equilibrium point.

Lemma A.2 *The origin of Eq. (26) is globally asymptotically stable if the system* $\dot{\boldsymbol{\eta}} = \boldsymbol{f}_0(\boldsymbol{\eta}, \boldsymbol{\xi})$ *is input-to-state stable.*

The proofs of Lemma A.1 and Lemma A.2 can be found in [2]. After the stability analyses of the *nominal system*, the stability of the perturbed system given by Eq. (25) is considered. Recall Eq. (11), the norm value of the perturbation term is

$$\|\boldsymbol{\delta}(\boldsymbol{x}, \Delta t)\|_2 = \|\boldsymbol{\delta}(z, \Delta t)|_{z=\boldsymbol{T}(\boldsymbol{x})}\|_2 = \|\frac{\partial[\boldsymbol{\alpha}(\boldsymbol{x}) + \mathcal{B}(\boldsymbol{x})\boldsymbol{u}]}{\partial \boldsymbol{x}}\Big|_0 \Delta\boldsymbol{x} + O(\Delta\boldsymbol{x}^2)\|_2 \tag{27}$$

Assume that all order partial derivatives of $\boldsymbol{\alpha}(\boldsymbol{x})$ and $\mathcal{B}(\boldsymbol{x})$ with respect to $\boldsymbol{x}$ are bounded. Due to the continuity of $\boldsymbol{x}$, $\lim_{\Delta t \to 0} \|\Delta\boldsymbol{x}\|_2 = 0$. Therefore, the perturbation term satisfies

$$\lim_{\Delta t \to 0} \|\boldsymbol{\delta}(z, \Delta t)\|_2 = 0, \quad \forall z \in \mathbb{R}^n \tag{28}$$

which means the norm value of this perturbation term become negligible for sufficiently high sampling frequency. Eq. (28) also indicates that $\forall\ \bar{\delta}_\varepsilon > 0, \exists\ \Delta\bar{t} > 0, s.t.$ for all $0 < \Delta t \le \Delta\bar{t}$, $\|\boldsymbol{\delta}(z, \Delta t)\|_2 \le \bar{\delta}_\varepsilon, \forall z \in \mathbb{R}^n, \forall t \ge t_0$. In other words, there exists a Δt that guarantees the boundedness of $\boldsymbol{\delta}(z, \Delta t)$. Also, this bound can be further diminished by increasing the sampling frequency.

Lemma A.3 *If* $\|\boldsymbol{\delta}(z, \Delta t)\|_2 \le \bar{\delta}_\varepsilon$ *is satisfied for all* $z \in \mathbb{R}^n$, *and* $\dot{\boldsymbol{\eta}} = \boldsymbol{f}_0(\boldsymbol{\eta}, \boldsymbol{\xi})$ *is input-to-state stable, then the state* z *of Eq. (25) is globally ultimately bounded by a class* $\mathcal{K}$ *function of* $\bar{\delta}_\varepsilon$.

Proof: Choose the candidate Lyapunov function as $V(\boldsymbol{\xi}) = \boldsymbol{\xi}^T\boldsymbol{P}\boldsymbol{\xi}$, where $\boldsymbol{P} = \boldsymbol{P}^T > 0$ is the solution of the Lyapunov equation $\boldsymbol{P}(\boldsymbol{A}_c - \boldsymbol{B}_c\boldsymbol{K}) + (\boldsymbol{A}_c - \boldsymbol{B}_c\boldsymbol{K})^T\boldsymbol{P} = -\boldsymbol{I}$, then $V(\boldsymbol{\xi})$ is positive definite and also satisfies

$$\begin{aligned} &\alpha_1(\|\boldsymbol{\xi}\|_2) \le V(\boldsymbol{\xi}) \le \alpha_2(\|\boldsymbol{\xi}\|_2) \\ &\alpha_1(\|\boldsymbol{\xi}\|_2) \triangleq \lambda_{min}(\boldsymbol{P})\|\boldsymbol{\xi}\|_2^2, \quad \alpha_2(\|\boldsymbol{\xi}\|_2) \triangleq \lambda_{max}(\boldsymbol{P})\|\boldsymbol{\xi}\|_2^2 \end{aligned} \tag{29}$$

$\lambda_{min}(\boldsymbol{P}), \lambda_{max}(\boldsymbol{P})$ are the minimum and maximum eigenvalues of the $\boldsymbol{P}$ matrix. α_1, α_2 belong to the class $\mathcal{K}_\infty$ functions. The partial derivative of the candidate Lyapunov function is calculated as

$$\begin{aligned}\dot{V} &= \boldsymbol{\xi}^T[\boldsymbol{P}(\boldsymbol{A}_c - \boldsymbol{B}_c\boldsymbol{K}) + (\boldsymbol{A}_c - \boldsymbol{B}_c\boldsymbol{K})^T\boldsymbol{P}]\boldsymbol{\xi} + 2\boldsymbol{\xi}^T\boldsymbol{P}\boldsymbol{B}_c\boldsymbol{\delta}(z, \Delta t) \\ &\leq -\|\boldsymbol{\xi}\|_2^2 + 2\|\boldsymbol{\xi}\|_2\|\boldsymbol{P}\boldsymbol{B}_c\|_2\bar{\delta}_\varepsilon \\ &\leq -\theta_1\|\boldsymbol{\xi}\|_2^2, \qquad \forall\|\boldsymbol{\xi}\|_2 \geq \frac{2\|\boldsymbol{P}\boldsymbol{B}_c\|_2\bar{\delta}_\varepsilon}{1-\theta_1} \triangleq \mu_1\bar{\delta}_\varepsilon \end{aligned} \tag{30}$$

with constant $\theta_1 \in (0, 1)$. Consequently, for $\forall\ \boldsymbol{\xi}(t_0) \in \mathbb{R}^\rho$, there exists a class $\mathcal{KL}$ function β and finite $T_1 \geq 0$ independent of t_0 such that $\|\boldsymbol{\xi}(t)\|_2$ satisfies [2]

$$\begin{aligned}\|\boldsymbol{\xi}(t)\|_2 &\leq \beta(\|\boldsymbol{\xi}(t_0)\|_2, t - t_0), \qquad t_0 \leq \forall\ t \leq t_0 + T_1 \\ \|\boldsymbol{\xi}(t)\|_2 &\leq \alpha_1^{-1}(\alpha_2(\mu_1\bar{\delta}_\varepsilon)), \qquad \forall\ t \geq t_0 + T_1 \triangleq t_0' \end{aligned} \tag{31}$$

The above equations indicate that the external state $\boldsymbol{\xi}$ is bounded for all $t \geq t_0$ and ultimately bounded with the ultimate bound $\Gamma\bar{\delta}_\varepsilon \triangleq \alpha_1^{-1}(\alpha_2(\mu_1\bar{\delta}_\varepsilon)) = \sqrt{\lambda_{max}(\boldsymbol{P})/\lambda_{min}(\boldsymbol{P})}\mu_1\bar{\delta}_\varepsilon$.

Moreover, by the definition of input-to-state stability, there exists a class $\mathcal{KL}$ function β_0 and a class $\mathcal{K}$ function γ_0 such that for $\forall\ \boldsymbol{\eta}(t_0') \in \mathbb{R}^{n-\rho}$ and bounded input $\boldsymbol{\xi}$, the internal state $\boldsymbol{\eta}$ satisfies

$$\begin{aligned}\|\boldsymbol{\eta}(t)\|_2 &\leq \beta_0(\|\boldsymbol{\eta}(t_0')\|_2, t - t_0') + \gamma_0(\sup_{t_0' \leq \tau \leq t}\|\boldsymbol{\xi}(\tau)\|_2) \\ &= \beta_0(\|\boldsymbol{\eta}(t_0')\|_2, t - t_0') + \gamma_0(\Gamma\bar{\delta}_\varepsilon) \end{aligned} \tag{32}$$

In addition, because β_0 belongs to class $\mathcal{KL}$ functions, then $\beta_0(\|\boldsymbol{\eta}(t_0')\|_2, t - t_0') \leq \theta_2\bar{\delta}_\varepsilon$, for some finite $T_2 > 0$ and $\theta_2 > 0$. Hence, the state $\boldsymbol{z}$ satisfies

$$\|z(t)\|_2 \leq \|\boldsymbol{\xi}(t)\|_2 + \|\boldsymbol{\eta}(t)\|_2 = (\Gamma + \theta_2)\bar{\delta}_\varepsilon + \gamma_0(\Gamma\bar{\delta}_\varepsilon), \quad \forall t \geq t_0 + T_1 + T_2 \tag{33}$$

which proves that $\boldsymbol{z}(t)$ is globally ultimately bounded by a class $\mathcal{K}$ function of $\bar{\delta}_\varepsilon$. □

Lemma A.3 has no restriction on the values of the initial state and the perturbation bound $\bar{\delta}_\varepsilon$. However, when the internal dynamics $\dot{\boldsymbol{\eta}} = \boldsymbol{f}_0(\boldsymbol{\eta}, \boldsymbol{\xi})$ is not input-to-state stable, but only the origin of the zero dynamics $\dot{\boldsymbol{\eta}} = \boldsymbol{f}_0(\boldsymbol{\eta}, \boldsymbol{0})$ is exponentially stable, then there will be restriction on the initial state, also the perturbations cannot be too large. These phenomena are presented in the next Lemma.

Lemma A.4 *If $\|\boldsymbol{\delta}(z, \Delta t)\|_2 \leq \bar{\delta}_\varepsilon$ is satisfied for all $\boldsymbol{z} \in \mathbb{R}^n$, and the origin of $\dot{\boldsymbol{\eta}} = \boldsymbol{f}_0(\boldsymbol{\eta}, \boldsymbol{0})$ is exponentially stable, then there is a neighborhood D_z of $\boldsymbol{z} = \boldsymbol{0}$ and $\varepsilon^* > 0$, such that for every $\boldsymbol{z}(0) \in D_z$ and $\bar{\delta}_\varepsilon < \varepsilon^*$, the state $\boldsymbol{z}$ of Eq. (25) is ultimately bounded by a class $\mathcal{K}$ function of $\bar{\delta}_\varepsilon$.*

Proof: According to the converse Lyapunov theorem [2], because the origin of $\dot{\boldsymbol{\eta}} = \boldsymbol{f}_0(\boldsymbol{\eta}, \boldsymbol{0})$ is exponentially stable, there exists a Lyapunov function $V_2(\boldsymbol{\eta})$ defined in $D_\eta = \{\boldsymbol{\eta} \in \mathbb{R}^{n-\rho} |\ \|\boldsymbol{\eta}\| < r_\eta\}$ satisfies the inequalities

$$c_1\|\boldsymbol{\eta}\|_2^2 \leq V_2(\boldsymbol{\eta}) \leq c_2\|\boldsymbol{\eta}\|_2^2, \quad \frac{\partial V_2}{\partial \boldsymbol{\eta}}\boldsymbol{f}_0(\boldsymbol{\eta}, \boldsymbol{0}) \leq -c_3\|\boldsymbol{\eta}\|_2^2, \quad \|\frac{\partial V_2}{\partial \boldsymbol{\eta}}\|_2 \leq c_4\|\boldsymbol{\eta}\|_2 \tag{34}$$

for some positive constants c_1, c_2, c_3, c_4. Denote

$$\alpha_1'(\|\boldsymbol{\eta}\|_2) \triangleq c_1\|\boldsymbol{\eta}\|_2^2, \quad \alpha_2'(\|\boldsymbol{\eta}\|_2) \triangleq c_2\|\boldsymbol{\eta}\|_2^2 \tag{35}$$

then α_1', α_2' belong to class $\mathcal{K}_\infty$ functions. Besides, because $\boldsymbol{f}_0$ is continuous and differentiable, there exists a Lipschitz constant L of $\boldsymbol{f}_0$ with respect to $\boldsymbol{\xi}$ such that

$$\|\boldsymbol{f}_0(\boldsymbol{\eta}, \boldsymbol{\xi}) - \boldsymbol{f}_0(\boldsymbol{\eta}, \boldsymbol{0})\|_2 \leq L\|\boldsymbol{\xi}\|_2, \quad \forall\|\boldsymbol{\eta}\| < r_\eta \tag{36}$$

Choose $V_2(\boldsymbol{\eta})$ as the candidate Lyapunov function for $\dot{\boldsymbol{\eta}} = \boldsymbol{f}_0(\boldsymbol{\eta}, \boldsymbol{\xi})$, with derivative

$$\begin{aligned}\dot{V}_2(\boldsymbol{\eta}) &= \frac{\partial V_2}{\partial \boldsymbol{\eta}}\boldsymbol{f}_0(\boldsymbol{\eta}, \boldsymbol{0}) + \frac{\partial V_2}{\partial \boldsymbol{\eta}}[\boldsymbol{f}_0(\boldsymbol{\eta}, \boldsymbol{\xi}) - \boldsymbol{f}_0(\boldsymbol{\eta}, \boldsymbol{0})] \\ &\leq -c_3\|\boldsymbol{\eta}\|_2^2 + c_4L\|\boldsymbol{\eta}\|_2\|\boldsymbol{\xi}\|_2 \\ &\leq -c_3(1-\theta_3)\|\boldsymbol{\eta}\|_2^2, \qquad \frac{c_4L\|\boldsymbol{\xi}\|_2}{c_3\theta_3} \leq \forall\|\boldsymbol{\eta}\|_2 \leq r_\eta \end{aligned} \tag{37}$$

with constant $\theta_3 \in (0,1)$. Denote

$$\mu \triangleq \frac{c_4 L}{c_3 \theta_3}(\sup_{t_0' \le \tau \le t} \|\boldsymbol{\xi}(\tau)\|_2) \triangleq \theta_5(\sup_{t_0' \le \tau \le t} \|\boldsymbol{\xi}(\tau)\|_2) \tag{38}$$

then

$$\dot{V}_2(\boldsymbol{\eta}) \le -c_3(1-\theta_3)\|\boldsymbol{\eta}\|_2^2, \quad \mu \le \forall \|\boldsymbol{\eta}\|_2 \le r_\eta, \quad \forall t \ge t_0' \tag{39}$$

Since the conditions for the external states $\boldsymbol{\xi}$ are the same as compared to Lemma A.3, Eqs. (29, 30, 31) also hold true in this Lemma. From Eq. (31), the supremum of the external state is given by

$$\sup_{t_0' \le \tau \le t} \|\boldsymbol{\xi}(\tau)\|_2 = \alpha_1^{-1}(\alpha_2(\mu_1 \bar{\delta}_\varepsilon)) \tag{40}$$

Take $0 < r < r_\eta$ such that $D_r \subset D_\eta$, according to the boundedness theories [2], if

$$\mu < \alpha_2'^{-1}(\alpha_1'(r)), \quad \|\boldsymbol{\eta}(t_0')\|_2 \le \alpha_2'^{-1}(\alpha_1'(r)) \tag{41}$$

then there exists a class $\mathcal{KL}$ function β_0' such that

$$\|\boldsymbol{\eta}(t)\|_2 \le \beta_0'(\|\boldsymbol{\eta}(t_0')\|_2, t - t_0') + \alpha_1'^{-1}(\alpha_2'(\mu)), \quad \forall t \ge t_0' \tag{42}$$

Eq. (41) proposes requirements on both the initial condition and the perturbation bound. Using Eqs. (38, 40, 41), the maximum perturbation that the system can sustain is given by

$$\bar{\delta}_\varepsilon < \varepsilon^* \triangleq (1/\mu_1)\alpha_2^{-1}(\alpha_1((1/\theta_5)\alpha_2'^{-1}(\alpha_1'(r)))) \tag{43}$$

From Eqs. (38, 40, 42), the normal value of the internal state yields

$$\begin{aligned} \|\boldsymbol{\eta}(t)\|_2 &\le \beta_0'(\|\boldsymbol{\eta}(t_0')\|_2, t - t_0') + \alpha_1'^{-1}(\alpha_2'(\theta_5 \alpha_1^{-1}(\alpha_2(\mu_1 \bar{\delta}_\varepsilon)))) \\ &\le \theta_6 \bar{\delta}_\varepsilon + \theta_5 \alpha_1'^{-1}(\alpha_2'(\alpha_1^{-1}(\alpha_2(\mu_1 \bar{\delta}_\varepsilon)))), \qquad \forall t \ge t_0 + T_1 + T_3 \end{aligned} \tag{44}$$

for some finite $T_3 > 0$ and $\theta_6 > 0$. Hence, state $\boldsymbol{z}$ satisfies

$$\begin{aligned} \|\boldsymbol{z}(t)\|_2 &\le \|\boldsymbol{\xi}(t)\|_2 + \|\boldsymbol{\eta}(t)\|_2 \\ &= (\Gamma + \theta_6)\bar{\delta}_\varepsilon + \theta_5 \alpha_1'^{-1}(\alpha_2'(\alpha_1^{-1}(\alpha_2(\mu_1 \bar{\delta}_\varepsilon)))), \quad \forall t \ge t_0 + T_1 + T_3 \end{aligned} \tag{45}$$

which proves the $\boldsymbol{z}(t)$ is ultimately bounded by a class $\mathcal{K}$ function of $\bar{\delta}_\varepsilon$. □

B. Robustness Analysis

1. Disturbance Rejection

The INDI control method has shown promising disturbance rejection ability in reference tracking problems and was verified by both simulations [15] and quad-rotor flight tests [13, 14]. It can also be designed to alleviate the structure loads and improve the ride quality in the presence of atmospheric turbulence and gusts [15]. However, by far, there lack of theoretical proof for the stability and boundedness of the closed-loop system using INDI control under the perturbation of external disturbances, these issues will be discussed in this subsection.

Normally, the external disturbances are bounded in real life, denote

$$\bar{d} \triangleq \sup\{\|\mathbf{d}(t)\|_2, \ \mathbf{d} \in \mathbb{R}^n\}, \quad \forall t \ge t_0 \tag{46}$$

which is independent of the sampling interval Δt. Different from the continuousness condition for $\boldsymbol{x}$, there is no requirement on the continuity of $\mathbf{d}$, it can be atmospheric turbulence or a sudden bird strike. When $\Delta t \to 0$, $\|\Delta \mathbf{d}\|_2$ does not necessarily verge to zero. However, for a given sampling rate, the supremum of $\|\Delta \mathbf{d}\|_2$ exists, denote

$$\bar{d}_\varepsilon(\Delta t) \triangleq \sup\{\|\Delta \mathbf{d}(t)\|_2, \ \Delta \mathbf{d} \in \mathbb{R}^n\}, \quad \forall t \ge t_0 \tag{47}$$

As a function of Δt, $\bar{d}_\varepsilon(\Delta t)$ can be reduced by increasing the sampling frequency. Recall the system modeled by Eqs. (23, 24), and design the pseudo-control as $\boldsymbol{\nu} = -\boldsymbol{K}\boldsymbol{\xi}$ to stabilize the origin $\boldsymbol{z} = [\boldsymbol{\eta}; \boldsymbol{\xi}] = \mathbf{0}$, the closed-loop system is then given by

$$\begin{aligned} \dot{\boldsymbol{\eta}} &= \boldsymbol{f}_d(\boldsymbol{\eta}, \boldsymbol{\xi}, \boldsymbol{d}) \\ \dot{\boldsymbol{\xi}} &= -\boldsymbol{K}\boldsymbol{\xi} + \boldsymbol{H}\Delta \boldsymbol{d} + \boldsymbol{\delta}(\boldsymbol{\xi}, \Delta t) \end{aligned} \tag{48}$$

Proposition B.1 *If $\|\boldsymbol{\delta}(\boldsymbol{\xi}, \Delta t)\|_2 \leq \bar{\delta}_\varepsilon$ is satisfied for all $\boldsymbol{\xi} \in \mathbb{R}^\rho$, $\dot{\boldsymbol{\eta}} = \boldsymbol{f}_d(\boldsymbol{\eta}, \boldsymbol{\xi}, \boldsymbol{d})$ is continuously differentiable and globally Lipschitz in $(\boldsymbol{\eta}, \boldsymbol{\xi}, \boldsymbol{d})$, and the origin of $\dot{\boldsymbol{\eta}} = \boldsymbol{f}_d(\boldsymbol{\eta}, \boldsymbol{0}, \boldsymbol{0})$ is globally exponentially stable, then the external state $\boldsymbol{\xi}$ and internal state $\boldsymbol{\eta}$ of Eq. (48) are globally ultimately bounded by a class $\mathcal{K}$ function of $\bar{\delta}_\varepsilon, \bar{d}_\varepsilon$ and a class $\mathcal{K}$ function of $\bar{d}, \bar{\delta}_\varepsilon, \bar{d}_\varepsilon$ respectively.*

Proof: The norm value of the perturbation term in Eq. (48) satisfies

$$\|\boldsymbol{H}\Delta\boldsymbol{d} + \boldsymbol{\delta}(\boldsymbol{\xi}, \Delta t)\|_2 \leq \|\boldsymbol{H}\|_2\|\Delta\boldsymbol{d}\|_2 + \|\boldsymbol{\delta}(\boldsymbol{\xi}, \Delta t)\|_2 = \bar{d}_\varepsilon + \bar{\delta}_\varepsilon \tag{49}$$

where $\|\boldsymbol{H}\|_2 = 1$ since $\boldsymbol{H}$ is a Boolean selection matrix. Similar to the proof of Lemma A.3, choose the candidate Lyapunov function as $V(\boldsymbol{\xi}) = \boldsymbol{\xi}^T\boldsymbol{P}\boldsymbol{\xi}$, where $\boldsymbol{P} = \boldsymbol{P}^T > 0$ is the solution of the Lyapunov equation $\boldsymbol{P}\boldsymbol{K} + \boldsymbol{K}^T\boldsymbol{P} = \boldsymbol{I}$, then the time derivatives of $V(\boldsymbol{\xi})$ satisfies

$$\dot{V} \leq -\theta_1\|\boldsymbol{\xi}\|_2^2, \qquad \forall\|\boldsymbol{\xi}\|_2 \geq \frac{2\|\boldsymbol{P}\|_2(\bar{\delta}_\varepsilon + \bar{d}_\varepsilon)}{1-\theta_1} \triangleq \mu_2(\bar{\delta}_\varepsilon + \bar{d}_\varepsilon) \tag{50}$$

Therefore, $\forall\ \boldsymbol{\xi}(t_0) \in \mathbb{R}^\rho$, there exists a class $\mathcal{KL}$ function β and $T_4 \geq 0$ independent of t_0 such that $\|\boldsymbol{\xi}(t)\|_2$ satisfies

$$\begin{aligned} \|\boldsymbol{\xi}(t)\|_2 &\leq \beta(\|\boldsymbol{\xi}(t_0)\|_2, t - t_0), \qquad t_0 \leq \forall\ t \leq t_0 + T_4 \\ \|\boldsymbol{\xi}(t)\|_2 &\leq \alpha_1^{-1}(\alpha_2(\mu_2(\bar{\delta}_\varepsilon + \bar{d}_\varepsilon))), \qquad \forall\ t \geq t_0 + T_4 \end{aligned} \tag{51}$$

In other words, the external states $\boldsymbol{\xi}$ is bounded for all $t \geq t_0$ and ultimately bounded with the ultimate bound $\Gamma_\xi \triangleq \alpha_1^{-1}(\alpha_2(\mu_2(\bar{\delta}_\varepsilon + \bar{d}_\varepsilon)))$, which is a class $\mathcal{K}$ function of $\bar{\delta}_\varepsilon$ and $\bar{d}_\varepsilon$.

On the other hand, perturbations directly acting on the internal dynamics. Because the origin of $\dot{\boldsymbol{\eta}} = \boldsymbol{f}_d(\boldsymbol{\eta}, \boldsymbol{0}, \boldsymbol{0})$ is globally exponentially stable, Eq. (34) is satisfied globally. Besides, since $\dot{\boldsymbol{\eta}} = \boldsymbol{f}_d(\boldsymbol{\eta}, \boldsymbol{\xi}, \boldsymbol{d})$ is continuously differentiable and globally Lipschitz in $(\boldsymbol{\eta}, \boldsymbol{\xi}, \boldsymbol{d})$, there exists a globally Lipschitz constant L such that

$$\|\boldsymbol{f}_d(\boldsymbol{\eta}, \boldsymbol{\xi}, \boldsymbol{d}) - \boldsymbol{f}_d(\boldsymbol{\eta}, \boldsymbol{0}, \boldsymbol{0})\|_2 \leq L(\|\boldsymbol{\xi}\|_2 + \|\boldsymbol{d}\|_2), \qquad \forall\boldsymbol{\eta} \in \mathbb{R}^{n-\rho} \tag{52}$$

Analogous to the proofs of Lemma A.4, Eq. (39) is satisfied for $\forall\|\boldsymbol{\eta}\|_2 \geq \mu'$ with $\mu' \triangleq \theta_5(\sup_{t_0+T_4\leq\tau\leq t}(\|\boldsymbol{\xi}(\tau)\|_2 + \|\boldsymbol{d}(\tau)\|_2))$, and the internal state $\|\boldsymbol{\eta}\|_2$ satisfies

$$\|\boldsymbol{\eta}(t)\|_2 \leq \beta_0'(\|\boldsymbol{\eta}(t_0 + T_4)\|_2, t - t_0 - T_4) + \theta_5\alpha_1'^{-1}(\alpha_2'(\Gamma_\xi + \bar{d})), \qquad \forall t \geq t_0 + T_4 \tag{53}$$

without restriction on the initial values and the disturbances bound. Due to the attenuation property of β_0'

$$\|\boldsymbol{\eta}(t)\|_2 \leq [\theta_7\bar{d} + \theta_5\alpha_1'^{-1}(\alpha_2'(\bar{d}))] + \theta_5\alpha_1'^{-1}(\alpha_2'(\alpha_1^{-1}(\alpha_2(\mu_2(\bar{\delta}_\varepsilon + \bar{d}_\varepsilon))))) \triangleq \Gamma_\eta, \quad \forall t \geq t_0 + T_4 + T_5 \tag{54}$$

for some $\theta_7 > 0$ and finite $T_5 > 0$. The above equation indicates that $\boldsymbol{\eta}$ is globally ultimately bounded by a class $\mathcal{K}$ function of $\bar{d}, \bar{\delta}_\varepsilon, \bar{d}_\varepsilon$. □

Remark: The estimation of the ultimate bounds could be conservative for a given perturbation term $\boldsymbol{H}\Delta\boldsymbol{d} + \boldsymbol{\delta}(\boldsymbol{\xi}, \Delta t)$, because the term $2\boldsymbol{\xi}^T\boldsymbol{P}\boldsymbol{B}_c\boldsymbol{\delta}(z, \Delta t)$ in Eq. (30) could be either positive or negative. Worse case analyses are done in Eq. (30) and Eq. (49) by taking the inequality constraints, which may lead to a conservative estimation of the ultimate bounds. The accurate ultimate bounds of a perturbed nonlinear system can be obtained via numerical simulations.

The disturbance rejection capability of a control method can be evaluated by the values of the ultimate bounds under prescribed disturbance perturbations. In view of Eqs. (51, 54), the ultimate bounds Γ_ξ and Γ_η are correlated to

1) System dynamics: Γ_ξ and Γ_η are functions of $\bar{\delta}_\varepsilon$, which is a gauge of the variation speed of the system dynamics as can be seen from Eq. (27). When the system dynamics are fast, which indicates $\|\frac{\partial[\boldsymbol{\alpha}(\boldsymbol{x})+\mathcal{B}(\boldsymbol{x})\boldsymbol{u}]}{\partial\boldsymbol{x}}|_0\|_2$ is large, the sampling frequency should be higher to ensure a desired ultimate bound. This has been verified by many application cases, for rigid airplane control, normally $f_s = 100$ Hz is enough [9, 11, 12, 15], while $f_s = 1000$ Hz is needed when the elastic modes of flexible aircraft are included. The sampling frequency used by quad-rotor UAV is $f_s = 512$ Hz [13, 14]. For the applications on hydraulic systems, $f_s = 5000$ Hz is desirable for controlling the hydraulic forces [16, 17].
2) Disturbance intensity: This can be seen from the expressions for Γ_ξ, Γ_η and definitions of $\bar{d}$, $\bar{d}_\varepsilon$, that stronger disturbances result into larger ultimate bounds.

3) $\boldsymbol{K}$ gains: As shown in Eqs. (51, 54), both Γ_ξ and Γ_η are monotonically increasing functions of μ_2. From Eq. (50) and the Lyapunov equation, it can be seen that larger $\boldsymbol{K}$ gains lead to smaller μ_2, and resulting in smaller ultimate bounds. Therefore, increasing $\boldsymbol{K}$ gains is beneficial for releasing the requirement on sampling frequency. As discussed before, the $\boldsymbol{K}$ gains are constrained by actuation system limits. High gain control would also amplify the measurement noise.
4) Sampling frequency: Recall Eqs. (28, 47), both $\bar{d}_\varepsilon$ and $\bar{\delta}_\varepsilon$ can be reduced by increasing the sampling frequency. When the sampling interval Δt is sufficiently small, $\|\Delta \boldsymbol{d}\| \leq \|\boldsymbol{d}\|$. The main part of the disturbances $\boldsymbol{d}_0$ and the model information can be reflected by the measurement of $\dot{\boldsymbol{\xi}}_0$ and compensated by the controller, thus resulting in marginal ultimate bounds. This is one feature that INDI distinguishes from Linear-Quadratic Regulator (LQR), Proportional-Integral (PI) and NDI control methods, where normally the disturbances can only be reflected in the measurement of states $\boldsymbol{\xi}$, which is a integration of $\dot{\boldsymbol{\xi}}_0$. Consequently, these control methods show inferior disturbance rejection ability as compared to the INDI method. In practice, the sampling frequency is constrained by the hardware.
5) Internal dynamics: It can be seen that the first term of Eq. (54) cannot be reduced by increasing the sampling frequency, and is a function of $\bar{d}$. This is because the internal dynamics are uncontrolled by the INDI method. Moreover, being inspired by Lemma A.4, when only the origin of $\dot{\boldsymbol{\eta}} = \boldsymbol{f}_d(\boldsymbol{\eta}, \boldsymbol{0}, \boldsymbol{0})$ is ensured to be exponentially stable or $\boldsymbol{f}_d$ is not globally Lipschitz, constrains on both the initial condition and the disturbance intensity need to be imposed to ensure the boundedness of states. This is presented as Corollary B.1. Therefore, the property of internal dynamics are important for the stability and robustness of the system.

Corollary B.1 *If $\|\boldsymbol{\delta}(\boldsymbol{\xi}, \Delta t)\|_2 \leq \bar{\delta}_\varepsilon$ is satisfied for all $\boldsymbol{\xi} \in \mathbb{R}^\rho$, and the origin of $\dot{\boldsymbol{\eta}} = \boldsymbol{f}_0(\boldsymbol{\eta}, \boldsymbol{0}, \boldsymbol{0})$ is exponentially stable, then there is a neighborhood D_z of $\boldsymbol{z} = \boldsymbol{0}$ and $\varepsilon^* > 0$, such that for every $\boldsymbol{z}(0) \in D_z$ and $(\bar{\delta}_\varepsilon + \bar{d}_\varepsilon) < \varepsilon^*$, the external state $\boldsymbol{\xi}$ and internal state $\boldsymbol{\eta}$ of Eq. (48) are ultimately bounded by a class $\mathcal{K}$ function of $\bar{\delta}_\varepsilon, \bar{d}_\varepsilon$ and a class $\mathcal{K}$ function of $\bar{d}, \bar{\delta}_\varepsilon, \bar{d}_\varepsilon$ respectively.*

The proof of Corollary B.1 is similar to the proofs of Proposition B.1 and Lemma A.4.

2. Robustness to Model Uncertainties

The model uncertainties considered in this section are classified into the *regular perturbations*, which are defined in the nonlinear system perturbation theory as the perturbations that do not change the order of the nominal system, such as negligible nonlinearities, parametric dispersions and variations. [5, 19].

There were few attempts on proofing the robustness of the INDI control method to aerodynamics model uncertainties, where it was proved by using linear transfer functions derived from block diagrams that the model mismatches of the control effectiveness matrix $\boldsymbol{G}(\boldsymbol{x})$ (or the generalized $\mathcal{B}(\boldsymbol{x})$) can be eliminated [9]. However, the assumption of $\dot{\boldsymbol{x}} = \dot{\boldsymbol{x}}_0$ is made in the block diagram, which is obviously incorrect since otherwise there will be no $\Delta \boldsymbol{u}$ term. Besides, the $\boldsymbol{\delta}(\boldsymbol{z}, \Delta t)$ term did not show up at all in previous proofs [9, 10, 13]. In view of these reasons, the robustness of INDI to model uncertainties will be rediscussed here.

Considering the nonlinear system with relative degree $\rho \leq n$ transformed into internal and external dynamics given by Eqs. (7, 8). The nominal NDI control to stabilize the system origin is given by

$$\boldsymbol{u}_n = \mathcal{B}^{-1}(\boldsymbol{x})(\boldsymbol{\nu} - \boldsymbol{\alpha}(\boldsymbol{x})) = \mathcal{B}^{-1}(\boldsymbol{x})(-\boldsymbol{K}\boldsymbol{T}_2(\boldsymbol{x}) - \boldsymbol{\alpha}(\boldsymbol{x})) \tag{55}$$

which requires the model knowledge of $\boldsymbol{\alpha}, \mathcal{B}, \boldsymbol{T}_2$ (defined in Eq. (7)). When the control law is applied using the approximated model as $\hat{\boldsymbol{\alpha}}, \hat{\mathcal{B}}, \hat{\boldsymbol{T}}_2$, the control input is given as

$$\boldsymbol{u}_{ndi} = \hat{\mathcal{B}}^{-1}(\boldsymbol{x})(-\boldsymbol{K}\hat{\boldsymbol{T}}_2(\boldsymbol{x}) - \hat{\boldsymbol{\alpha}}(\boldsymbol{x})) \tag{56}$$

and resulting in a closed-loop system as

$$\begin{aligned}
\dot{\boldsymbol{\eta}} &= \boldsymbol{f}_0(\boldsymbol{\eta}, \boldsymbol{\xi}) \\
\dot{\boldsymbol{\xi}} &= \boldsymbol{A}_c\boldsymbol{\xi} + \boldsymbol{B}_c[\boldsymbol{\alpha}(\boldsymbol{x}) + \mathcal{B}(\boldsymbol{x})\hat{\mathcal{B}}^{-1}(\boldsymbol{x})(-\boldsymbol{K}\hat{\boldsymbol{T}}_2(\boldsymbol{x}) - \hat{\boldsymbol{\alpha}}(\boldsymbol{x}))] \\
&= [\boldsymbol{A}_c\boldsymbol{\xi} - \boldsymbol{B}_c\boldsymbol{K}\hat{\boldsymbol{T}}_2(\boldsymbol{x})] + \boldsymbol{B}_c(\boldsymbol{\alpha}(\boldsymbol{x}) - \hat{\boldsymbol{\alpha}}(\boldsymbol{x})) + \boldsymbol{B}_c(\mathcal{B}(\boldsymbol{x})\hat{\mathcal{B}}^{-1}(\boldsymbol{x}) - \boldsymbol{I})(-\boldsymbol{K}\hat{\boldsymbol{T}}_2(\boldsymbol{x}) - \hat{\boldsymbol{\alpha}}(\boldsymbol{x})) \\
&= (\boldsymbol{A}_c - \boldsymbol{B}_c\boldsymbol{K})\boldsymbol{\xi} + \boldsymbol{B}_c\boldsymbol{K}(\boldsymbol{T}_2 - \hat{\boldsymbol{T}}_2) + \boldsymbol{B}_c(\boldsymbol{\alpha} - \hat{\boldsymbol{\alpha}}) + \boldsymbol{B}_c(\mathcal{B}\hat{\mathcal{B}}^{-1} - \boldsymbol{I})(-\boldsymbol{K}\hat{\boldsymbol{T}}_2 - \hat{\boldsymbol{\alpha}})
\end{aligned} \tag{57}$$

where $\boldsymbol{I} \in \mathbb{R}^{m\times m}$ is an identity matrix. As compared to the *nominal system* given by Eq. (26), this closed-loop system has three perturbation terms. Using Eq. (12), the nominal INDI control for stabilization is given by

$$\Delta \boldsymbol{u}_{in} = \mathcal{B}(\boldsymbol{x}_0)^{-1}(-\boldsymbol{K}\boldsymbol{T}_2(\boldsymbol{x}) - \boldsymbol{y}_0^{(\boldsymbol{\rho})}) \tag{58}$$

when applied using estimated model as

$$\Delta \boldsymbol{u}_{indi} = \hat{\mathcal{B}}(\boldsymbol{x}_0)^{-1}(-\boldsymbol{K}\hat{\boldsymbol{T}}_2(\boldsymbol{x}) - \boldsymbol{y}_0^{(\boldsymbol{\rho})}) \tag{59}$$

The closed-loop system under INDI control is

$$\begin{aligned} \dot{\boldsymbol{\eta}} &= \boldsymbol{f}_0(\boldsymbol{\eta}, \boldsymbol{\xi}) \\ \dot{\boldsymbol{\xi}} &= (\boldsymbol{A}_c - \boldsymbol{B}_c\boldsymbol{K})\boldsymbol{\xi} + \boldsymbol{B}_c\boldsymbol{K}(\boldsymbol{T}_2 - \hat{\boldsymbol{T}}_2) + \boldsymbol{B}_c\boldsymbol{\delta}(z, \Delta t) + \boldsymbol{B}_c(\mathcal{B}\hat{\mathcal{B}}^{-1} - \boldsymbol{I})(-\boldsymbol{K}\hat{\boldsymbol{T}}_2 - \boldsymbol{y}_0^{(\boldsymbol{\rho})}) \end{aligned} \tag{60}$$

The perturbation term $\boldsymbol{B}_c\boldsymbol{K}(\boldsymbol{T}_2 - \hat{\boldsymbol{T}}_2)$ is identical to the first perturbation term in Eq. (57). Since INDI control based on the measurements or estimations of $\boldsymbol{y}_0^{(\boldsymbol{\rho})}$ instead of the dynamic model $\boldsymbol{\alpha}(\boldsymbol{x})$, then the model uncertainty term $\boldsymbol{B}_c(\boldsymbol{\alpha}(\boldsymbol{x}) - \hat{\boldsymbol{\alpha}}(\boldsymbol{x}))$ is replaced by $\boldsymbol{B}_c\boldsymbol{\delta}(z, \Delta t)$ in INDI control. The influences of $\boldsymbol{\delta}(z, \Delta t)$ become negligible when the sampling frequency is high as indicated by Eq. (28).

The last term of Eqs. (57, 60) are mainly caused by the multiplicative uncertainties of the $\mathcal{B}(\boldsymbol{x})$ matrix. The last term of Eq. (60) was incorrectly omitted in literature [9, 10, 13, 14], so the present paper will show that although this term is a nonvanishing perturbation, its norm value is smaller than the norm value of the perturbation term under NDI control. Moreover, its influences can be further weakened by decreasing Δt.

Using the expression of $\Delta \boldsymbol{u}_{indi}$, the last term in Eq. (60) is given by

$$\boldsymbol{B}_c(\mathcal{B}\hat{\mathcal{B}}^{-1} - \boldsymbol{I})(-\boldsymbol{K}\hat{\boldsymbol{T}}_2 - \boldsymbol{y}_0^{(\boldsymbol{\rho})}) = \boldsymbol{B}_c(\mathcal{B}\hat{\mathcal{B}}^{-1} - \boldsymbol{I})\hat{\mathcal{B}}\Delta \boldsymbol{u}_{indi} = \boldsymbol{B}_c(\mathcal{B} - \hat{\mathcal{B}})\Delta \boldsymbol{u}_{indi} \tag{61}$$

with norm value $\|\mathcal{B} - \hat{\mathcal{B}}^{-1}\|\|\Delta \boldsymbol{u}_{indi}\|$, which can be reduced by increasing the sampling rate. On the contrary, using the expression for $\boldsymbol{u}_{ndi}$, the last term in Eq. (57) is given by

$$\boldsymbol{B}_c(\mathcal{B}\hat{\mathcal{B}}^{-1} - \boldsymbol{I})(-\boldsymbol{K}\hat{\boldsymbol{T}}_2 - \hat{\boldsymbol{\alpha}}) = \boldsymbol{B}_c(\mathcal{B}\hat{\mathcal{B}}^{-1} - \boldsymbol{I})\hat{\mathcal{B}}\boldsymbol{u}_{ndi} = \boldsymbol{B}_c(\mathcal{B} - \hat{\mathcal{B}})\boldsymbol{u}_{ndi} \tag{62}$$

with norm value $\|\mathcal{B} - \hat{\mathcal{B}}\|\|\boldsymbol{u}_{ndi}\|$, which is independent of Δt and normally larger than $\|\mathcal{B} - \hat{\mathcal{B}}\|\|\Delta \boldsymbol{u}_{indi}\|$.

In summary, in the presence of model uncertainties, the norm value of the perturbation terms in the closed-loop system under INDI control is smaller than that under NDI control, and can be further diminished by increasing the sampling frequency. As a result, according to Lemma A.3, when the internal dynamics $\dot{\boldsymbol{\eta}} = \boldsymbol{f}_0(\boldsymbol{\eta}, \boldsymbol{\xi})$ is input-to-state stable, the system using INDI control will result in smaller ultimate bounds. Besides, when only the origin of $\dot{\boldsymbol{\eta}} = \boldsymbol{f}_0(\boldsymbol{\eta}, \boldsymbol{0})$ is exponentially stable, system under the INDI control is easier to fulfill the boundedness condition $\bar{\delta}_\varepsilon < \varepsilon^*$ as demonstrated by Lemma A.4.

3. Sensing and Singular Perturbations

The presented INDI control has shown promising inherent robustness to disturbances and the regular perturbations without using any robust or adaptive control technique. There are other sources of perturbations that increase the order of the system, such as actuator dynamics and higher-order elastic dynamics. These perturbations are classified into *Singular perturbations* [5, 19]. Consider the singularly perturbed system model as [2]

$$\dot{\boldsymbol{x}} = \boldsymbol{f}(t, \boldsymbol{x}, \boldsymbol{z}_p, \epsilon), \qquad \epsilon\dot{\boldsymbol{z}}_p = \boldsymbol{g}_z(t, \boldsymbol{x}, \boldsymbol{z}_p, \epsilon) \tag{63}$$

where the perturbed dynamics are decomposed into reduced (slow) and boundary-layer (fast) dynamics. According to the Tikhonov's theorem [2], when the null (quasi) equilibrium states of both the fast and slow dynamics are exponentially stable, there exists a constant $\epsilon_{max} > 0$ such that the null equilibrium of the singularly perturbed system is exponentially stable for all $\epsilon < \epsilon_{max}$. This parameter $\epsilon_{max} > 0$ is referred to as the Singular Perturbation Margin (SPM) in literature [19], and is an equivalent to the Phase Margin (PM) of the Linear Time Invariant (LTI) systems in the sense of bijective function [19].

Regarding the applications of INDI to aerospace system angular rate control problems, the sensing of angular accelerations is needed. The angular accelerometer is already available in market, and a commonly used alternative

way to obtain the angular accelerations is by differentiating the filtered angular rate signals [10–17]. There have been legitimate concerns about the stability issue of this approach, and based on the above discussions, the system is able to sustain sufficiently small lags caused by filtering and actuator dynamics. This proposes an interesting research question of enlarging the SPM of the closed-loop system. Possible solutions could be using predictive filters [9] or actuator compensator [20]. This research question will be further studied in future work.

IV. Numerical Example

Since there have been extensive numerical applications of aircraft [9, 15], helicopter [10], micro air vehicle [13] and spacecraft [12] angular velocity control using INDI as the inner loop controller, this control structure will not be repeated here. The numerical example in this section consider a rigid aircraft Gust Load Alleviation (GLA) problem, where the vertical velocity is included in the inner loop INDI controller, provided the symmetrical aileron deflection is available. This idea originated from [15], but this old INDI derivation also has the blemishes mentioned before. Therefore, this problem will be resolved here.

The six Degrees of Freedom (6DoF) rigid aircraft dynamic equations of motion defined in the body frame is given by

$$\dot{\boldsymbol{V}}_f = -\boldsymbol{\omega} \times \boldsymbol{V}_f + \frac{\boldsymbol{F}}{m}, \quad \dot{\boldsymbol{\omega}} = -\boldsymbol{J}^{-1}\boldsymbol{\omega} \times \boldsymbol{J}\boldsymbol{\omega} + \boldsymbol{J}^{-1}\boldsymbol{M} \tag{64}$$

where $\boldsymbol{V}_f = [V_x, V_y, V_z]^T$ indicates the velocity of the aircraft c.g. relative to the inertial axis expressed in the body axis, and $\boldsymbol{\omega} = [p, q, r]^T$ represents the angular velocity. m is the total mass and $\boldsymbol{J}$ is the inertia matrix. $\boldsymbol{F}$ and $\boldsymbol{M}$ are the total forces and moments, which include the thrust, gravitational, control and aerodynamic forces and moments. The aerodynamic forces and moments are perturbed by the atmospheric disturbances. Considering an aircraft flying through a 2D symmetrical moderate vertical von Kármán turbulence field, with the turbulence velocity on each aerodynamic strip independently given by $\mathbf{V}_w$. The aircraft is flying through the turbulence field gradually, so that the gust velocities on the tail is delayed as compared to the gust velocities on the wing, expressed as $\mathbf{V}_{g_H} = e^{-\tau s}\mathbf{V}_{g_w}$, this setup allows the gust penetration effect to be included. The configuration and parameters of this aircraft can be found in [15].

The state vector is given as $\boldsymbol{x} = [V_x, V_y, V_z, p, q, r]^T$ with control inputs $\boldsymbol{u} = [\delta_e, \delta_r, \delta_{ar}, \delta_{al}]^T$ denoting the elevator, rudder, right and left aileron deflections respectively. Define the outputs as $\boldsymbol{y} = [V_z, p, q, r]^T$ and consider the output tracking problem. Based on the derivations in Sec. II, the system is decoupled into four control channels with relative degree one for each channel. Using Eqs. (18, 19, 23, 24) the INDI control law and resulting closed-loop system under external disturbance perturbations is given by

$$\begin{aligned} \Delta\boldsymbol{u} &= \mathcal{B}(\boldsymbol{x}_0)^{-1}[-\boldsymbol{K}\boldsymbol{e} - \boldsymbol{y}_0^{(\boldsymbol{\rho})} + \boldsymbol{r}^{(\boldsymbol{\rho})}] \\ \dot{\boldsymbol{\eta}} &= \boldsymbol{f}_d(\boldsymbol{\eta}, \boldsymbol{e} + \mathcal{R}, \boldsymbol{d}), \quad \dot{\boldsymbol{e}} = (\boldsymbol{A}_c - \boldsymbol{B}_c\boldsymbol{K})\boldsymbol{e} + \boldsymbol{H}\Delta\boldsymbol{d} + \boldsymbol{B}_c\boldsymbol{\delta}(z, \Delta t) \end{aligned} \tag{65}$$

External states $\boldsymbol{\xi} = \boldsymbol{y}$ according to Eq. (21) and there are two dimensional internal dynamics in this closed-loop system. Although the input-to-state stability of the internal dynamics is not easy to prove, the analysis of the origin stability of $\boldsymbol{f}_d(\boldsymbol{\eta}, \boldsymbol{0}, \boldsymbol{0})$ is practical. The two dimensional submanifold for the zero dynamics is given by

$$\boldsymbol{Z}^* = \{\boldsymbol{x} \in \mathbb{R}^6, \quad V_z = p = q = r = 0\} \tag{66}$$

Define $\boldsymbol{A}(t) = \frac{\partial \boldsymbol{f}_d}{\partial \boldsymbol{\eta}}|_{\boldsymbol{\eta}=\boldsymbol{0}}$, then $\boldsymbol{\eta} = \boldsymbol{0}$ is an exponentially stable equilibrium point of $\boldsymbol{f}_d$ if and only if it is an exponentially stable equilibrium point of the linear system $\dot{\boldsymbol{\eta}} = \boldsymbol{A}(t)\boldsymbol{\eta}$ [2]. This allows the origin stability of the zero dynamics been easily tested via linearization. The origin of $\dot{\boldsymbol{\eta}} = \boldsymbol{f}_d(\boldsymbol{\eta}, \boldsymbol{0}, \boldsymbol{0})$ has been tested to be exponentially stable for this model, otherwise, additional thrust control loop with velocity feedback and side-slip angle control loop using rudder can guarantee the stability of $\boldsymbol{\eta}$ for 6DoF aerospace systems.

According to Corollary B.1, the $\boldsymbol{\eta}$ and reference tracking error $\boldsymbol{e}$ can then be concluded to be ultimately bounded under small perturbations. Moreover, the ultimate bounds have been proved to be monotonically decreasing functions of $\boldsymbol{K}$ gains and the sampling frequency in Sec. III. The following simulation will test the fidelity of these conclusions when actuator dynamics and limits are considered.

Set the references for $[V_z, p, r]^T$ to be their trim values $[V_z^*, 0, 0]^T$, and the reference signal for q is designed as a sinusoid single with magnitude of 1.5°/s and frequency of 1.5 Hz. Setting the initial condition as $\boldsymbol{x}(t = 0) = [0.5$ m/s, 0°/s, 2°/s, 0°/s$]^T$, and design the gain matrix as $\boldsymbol{K} = a \cdot \boldsymbol{I}_{4\times4}$. All the control surfaces are modeled as first order systems with transfer function $A(s) = \frac{20}{s+20}$. The deflection limits of ailerons, elevator and rudder are ±35°, ±25°, ±25°

respectively. The rate limit for ailerons is 100°/s and is 60°/s for elevator and rudder. The simulation frequency (difference from sampling frequency) is 2000 Hz, which is chosen to be sufficiently high to simulate the property of the continuous dynamics in the real life. There are three sampling processes in this control law, namely the measurement of the outputs $\dot{\boldsymbol{y}}_0$, $\boldsymbol{y}_0$ and the actuator position $\boldsymbol{u}_0$. The sampling frequency varies in the subsequent analyses. The block diagram illustrate this control law considering the actuator dynamics is given by Fig. 1. The simulation results are shown as Figs. 2-5.

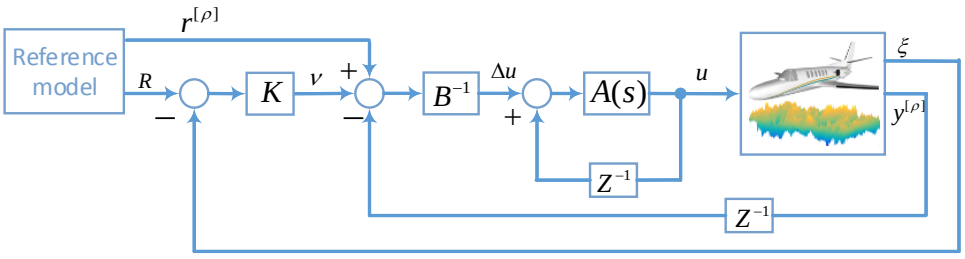

Fig. 1 The block diagram for reference tracking problem applied with actuator dynamics.

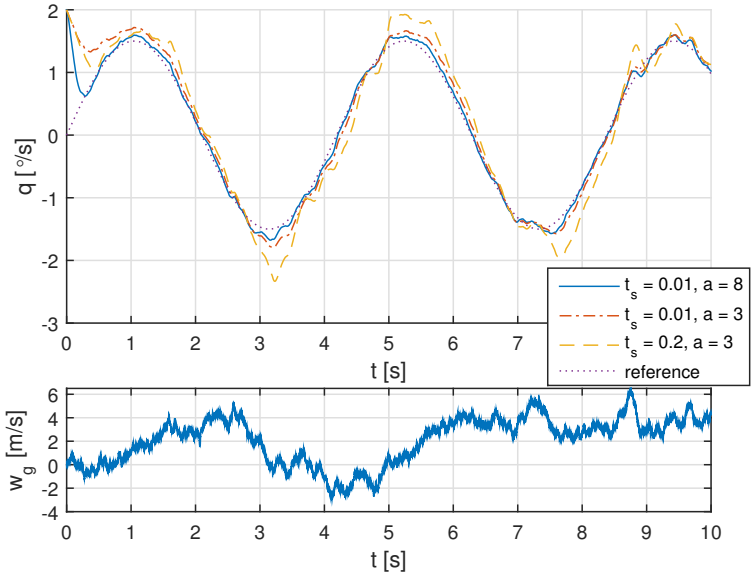

Fig. 2 Pitch rate tracking responses and turbulence input.

As can be seen from Fig. 2, under all sets of controller parameters, the aircraft is able to track the pitch rate command. When $a = 3$, the ultimate bounds for $\Delta t = 0.01$ s is $|e_{V_z}| = 0.23$ m/s, $|e_q| = 0.30$°/s and degrade into larger ultimate bounds of $|e_{V_z}| = 0.68$ m/s, $|e_q| = 0.85$°/s when the sampling interval increased into $\Delta t = 0.2$ s, these phenomena are illustrated by Fig. 3. Under the same sampling interval $\Delta t = 0.01$ s, when the outer loop gains increased from $\boldsymbol{K} = 3 \cdot \boldsymbol{I}_{4\times4}$ to $\boldsymbol{K} = 8 \cdot \boldsymbol{I}_{4\times4}$, the closed-loop system responses faster to the errors, and results into smaller ultimate bounds, as shown in Fig. 2 and Fig. 3. The control surface deflections are illustrated by Fig. 4.

Fig. 5 shows the ultimate bounds of e_{V_z} and e_q using various controller parameters. The tested sampling intervals varies from $\Delta t = 0.001$ s to $\Delta t = 0.2$ s. As can be seen from Fig. 5, in general, for a given gain matrix $\boldsymbol{K} = a \cdot \boldsymbol{I}_{4\times4}$, the ultimate bounds decrease as the sampling interval decreases. This trend of decrease becomes slower around $\Delta t = 0.12$ s as the contour lines become sparser. Further decreasing the sampling interval does improve the performance but would impose higher requirements on the hardware.

On the other hand, for a given Δt, as a increases from $a = 1$ to $a = 13$, the ultimate bounds decreases first, reaches a minimum around $a \approx 8$, then shows a trend of increase as a further increases. As analyzed before, the ultimate

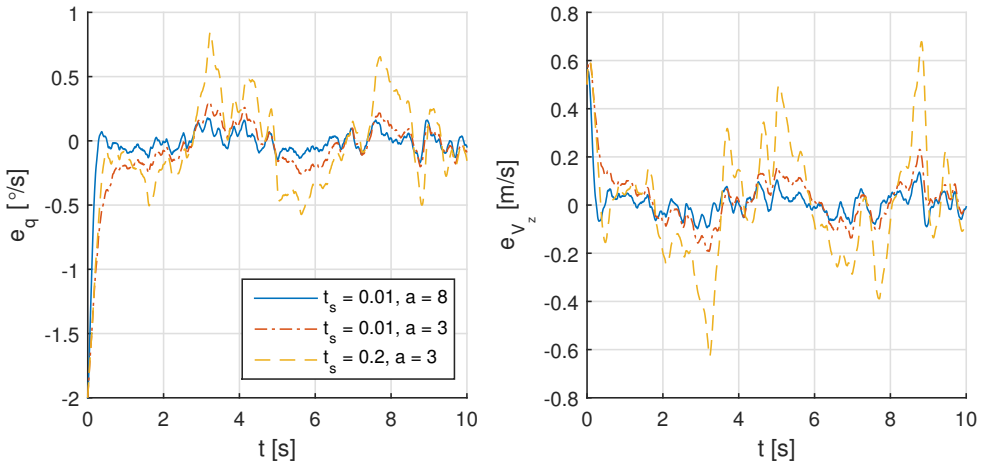

Fig. 3 Tracking error responses.

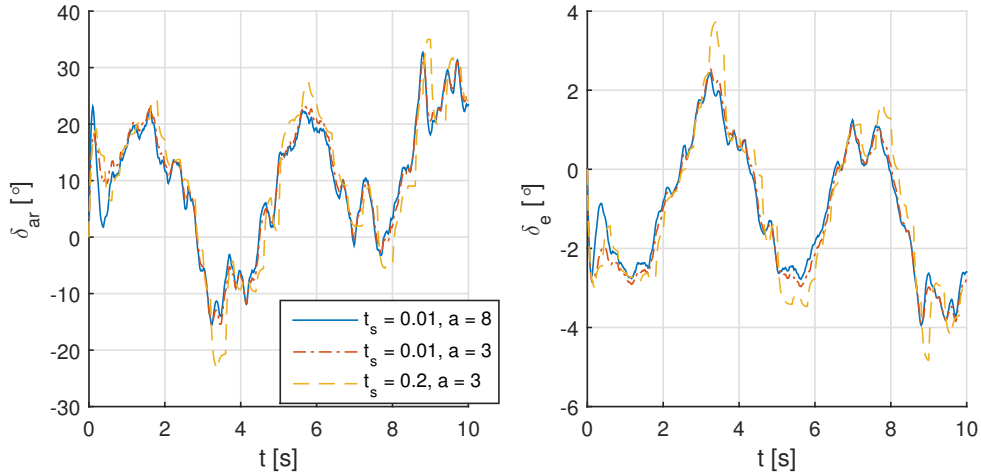

Fig. 4 Control surface deflections.

bounds will be smaller for larger $\boldsymbol{K}$ gains when ideal actuators are applied. However, larger gains would amplify the measurement noise and lead to control surfaces saturations in practice, which degrade the performance for $a > 8$ and potentially lead to divergence.

This simulation verified the ultimate boundedness of the states especially when the actuator dynamics and limits are considered. The influences of $\boldsymbol{K}$ gains and the sampling frequency on the ultimate bounds are also verified.

V. Conclusions

In this paper, the INDI control law is reformulated without using the time scale separation principle. Three problems, namely the input-output linearization, output tracking and input-to-state linearization in the presence of external disturbances are considered, where INDI is generalized into not necessarily relative-degree-one problem with consideration of the internal dynamics.

Using Lyapunov methods and nonlinear system perturbation theory, the stability of the closed-loop system using INDI is then analyzed. It is proved that the norm value of the INDI perturbation term converges to zero when the sampling interval trends to zero. The state of the closed-loop system is proved to be ultimately bounded by a class $\mathcal{K}$ function of the perturbation bounds. There is no restriction of the perturbation value and the initial condition if the internal dynamics is input-to-state stable (Lemma A.3). Otherwise, corresponding restrictions would appear as shown

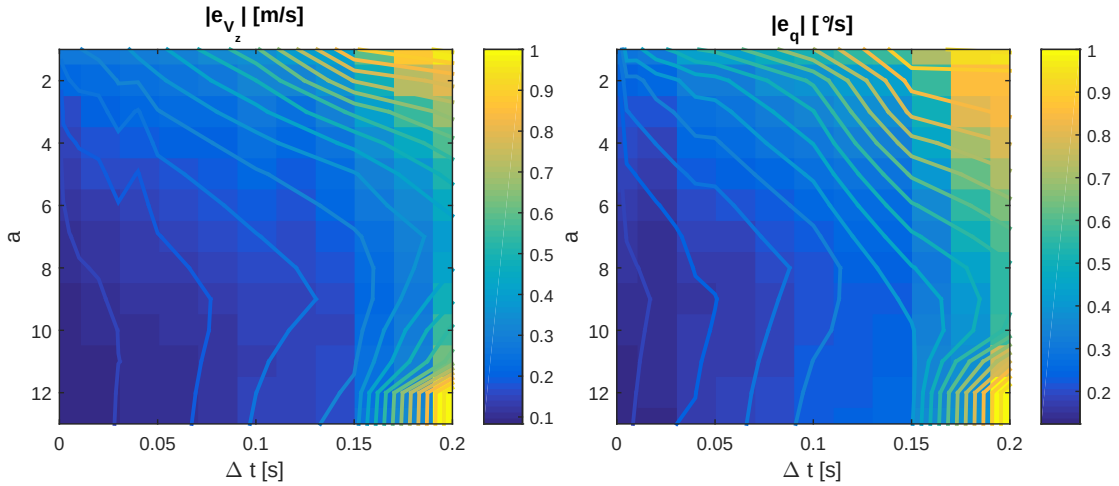

Fig. 5 The influences of sampling interval and outer loop gains on the ultimate bounds.

in Lemma A.4.

Moreover, in the presence of external disturbances, both the internal and external states of the closed-loop system are proved to be ultimately bounded by class $\mathcal{K}$ functions (Proposition B.1, Corollary B.1). Disturbances are shown to directly perturb the internal dynamics while perturb the external dynamics only by their increments, which is the reason for the better disturbance rejection capability of the INDI method. The influences of the system dynamics, disturbance intensity, $\boldsymbol{K}$ gains, sampling frequency and the internal dynamics property on the values of ultimate bounds are also analyzed.

Besides, the robustness of the closed-loop system to regular and singular perturbations are analyzed. The INDI control method was proved to have better robust performance under regular perturbations as compared to NDI without using any robust or adaptive techniques. It can also resists certain region of singular perturbations.

Finally, the reformulated INDI control law is numerically verified by a rigid aircraft Gust Load Alleviation (GLA) problem. The reference tracking errors are shown to be ultimately bounded when the INDI control law is applied considering actuator dynamics and limits. The influences of the $\boldsymbol{K}$ gains and sampling frequency on the values of the ultimate bounds are also demonstrated.

In conclusion, this reformulated INDI control law is promising for solving aerospace system control problems. The way to enlarger the Singular Perturbation Margin (SPM [19]) of INDI can be recommended as future work.

References

[1] Slotine, J.-J. E., and Li, W., *Applied Nonlinear Control*, NJ: Prentice hall, Englewood Cliffs, 1991.

[2] Khalil, H. K., *Nonlinear Systems*, Prentice-Hall, New Jersey, 2002.

[3] Reiner, J., Balas, G. J., and Garrard, W. L., "Flight control design using Robust dynamic inversion and time-scale separation," *Automatica*, Vol. 32, No. 11, 1996, pp. 1493–1504. doi:10.1016/S0005-1098(96)00101-X.

[4] Lee, H., Reiman, S., Dillon, C., and Youssef, H., "Robust Nonlinear Dynamic Inversion Control for a Hypersonic Cruise Vehicle," *AIAA Guidance, Navigation, and Control Conference and Exhibit*, 2007, pp. 1–10. doi:10.2514/6.2007-6685, URL `http://arc.aiaa.org/doi/pdf/10.2514/6.2007-6685`.

[5] Hodel, A., Whorton, M., and Zhu, J., "Stability Metrics for Simulation and Flight-Software Assessment and Monitoring of Adaptive Control Assist Compensators," *AIAA Guidance, Navigation and Control Conference and Exhibit*, American Institute of Aeronautics and Astronautics, Honolulu, Hawaii, 2008, pp. 1–25. doi:10.2514/6.2008-7005, URL `http://arc.aiaa.org/doi/10.2514/6.2008-7005`.

[6] Lombaerts, T., "Fault Tolerant Flight Control, A Physical Model Approach," Ph.D. thesis, Delft University of Technology, 2010.

[7] Smith, P., "A Simplified Approach to Nonlinear Dynamic Inversion Based Flight Control," *23rd Atmospheric Flight Mechanics Conference*, American Institute of Aeronautics and Astronautics, Reston, VA, 1998. doi:10.2514/6.1998-4461, URL http://arc.aiaa.org/doi/10.2514/6.1998-4461.

[8] Bacon, B., Ostroff, A., and Joshi, S., "Reconfigurable NDI controller using inertial sensor failure detection & isolation," *IEEE Transactions on Aerospace and Electronic Systems*, Vol. 37, No. 4, 2001, pp. 1373–1383. doi:10.1109/7.976972, URL http://ieeexplore.ieee.org/document/976972/.

[9] Sieberling, S., Chu, Q. P., and Mulder, J. A., "Robust Flight Control Using Incremental Nonlinear Dynamic Inversion and Angular Acceleration Prediction," *Journal of Guidance, Control, and Dynamics*, Vol. 33, No. 6, 2010, pp. 1732–1742. doi:10.2514/1.49978, URL http://arc.aiaa.org/doi/abs/10.2514/1.49978.

[10] Simplício, P., Pavel, M., van Kampen, E., and Chu, Q., "An acceleration measurements-based approach for helicopter nonlinear flight control using Incremental Nonlinear Dynamic Inversion," *Control Engineering Practice*, Vol. 21, No. 8, 2013, pp. 1065–1077. doi:10.1016/j.conengprac.2013.03.009, URL http://dx.doi.org/10.1016/j.conengprac.2013.03.009.

[11] Lu, P., van Kampen, E.-J., de Visser, C., and Chu, Q., "Aircraft fault-tolerant trajectory control using Incremental Nonlinear Dynamic Inversion," *Control Engineering Practice*, Vol. 57, 2016, pp. 126–141. doi:10.1016/j.conengprac.2016.09.010, URL http://dx.doi.org/10.1016/j.conengprac.2016.09.010.

[12] Acquatella, P., Falkena, W., van Kampen, E.-J., and Chu, Q. P., "Robust Nonlinear Spacecraft Attitude Control using Incremental Nonlinear Dynamic Inversion." *AIAA Guidance, Navigation, and Control Conference*, American Institute of Aeronautics and Astronautics, Minneapolis, Minnesota, 2012. doi:10.2514/6.2012-4623, URL http://arc.aiaa.org/doi/10.2514/6.2012-4623.

[13] Smeur, E. J. J., Chu, Q. P., and de Croon, G. C. H. E., "Adaptive Incremental Nonlinear Dynamic Inversion for Attitude Control of Micro Air Vehicles," *Journal of Guidance, Control, and Dynamics*, Vol. 39, No. 3, 2016, pp. 450–461. doi:10.2514/1.G001490, URL http://arc.aiaa.org/doi/10.2514/1.G001490.

[14] Smeur, E. J., de Croon, G. C., and Chu, Q., "Gust Disturbance Alleviation with Incremental Nonlinear Dynamic Inversion," *2016 IEEE/RSJ International Conference on Intelligent Robots and Systems (IROS)*, IEEE, 2016, pp. 5626–5631. doi:10.1109/IROS.2016.7759827, URL http://ieeexplore.ieee.org/document/7759827/.

[15] Wang, X., Van Kampen, E.-J., and Chu, Q. P., "Gust Load Alleviation and Ride Quality Improvement with Incremental Nonlinear Dynamic Inversion," *AIAA Atmospheric Flight Mechanics Conference*, American Institute of Aeronautics and Astronautics, Grapevine, Texas, 2017, pp. 1–21. doi:10.2514/6.2017-1400, URL http://arc.aiaa.org/doi/10.2514/6.2017-1400.

[16] Huang, Y., Pool, D. M., Stroosma, O., Chu, Q. P., and Mulder, M., "A Review of Control Schemes for Hydraulic Stewart Platform Flight Simulator Motion Systems," *AIAA Modeling and Simulation Technologies Conference*, American Institute of Aeronautics and Astronautics, San Diego, California, 2016, pp. 1–14. doi:10.2514/6.2016-1436, URL http://arc.aiaa.org/doi/10.2514/6.2016-1436.

[17] Huang, Y., Pool, D. M., Stroosma, O., and Chu, Q. P., "Incremental Nonlinear Dynamic Inversion Control for Hydraulic Hexapod Flight Simulator Motion Systems," *IFAC-PapersOnLine*, Vol. 50, No. 1, 2017, pp. 4378–4383. doi:10.1016/j.ifacol.2017.08.837, URL https://doi.org/10.1016/j.ifacol.2017.08.837.

[18] Fradkov, A. L., Miroshnik, I. V., and Nikiforov, V. O., *Nonlinear and adaptive control of complex systems*, Vol. 491, Springer Science & Business Media, 2013.

[19] Yang, X., and Zhu, J. J., "Singular perturbation margin and generalised gain margin for nonlinear time-invariant systems," *International Journal of Control*, Vol. 89, No. 3, 2016, pp. 451–468. doi:10.1080/00207179.2015.1079738, URL http://www.tandfonline.com/doi/full/10.1080/00207179.2015.1079738.

[20] Lu, P., Van Kampen, E.-J., and Chu, Q., "Robustness and Tuning of Incremental Backstepping Approach," *AIAA Guidance, Navigation, and Control Conference*, American Institute of Aeronautics and Astronautics, Kissimmee, Florida, 2015, pp. 1–15. doi:10.2514/6.2015-1762, URL http://arc.aiaa.org/doi/10.2514/6.2015-1762.